Failure mode analysis of lead rubber bearings and CFST column series isolation system

Zhongtie Wu[a*], Cheng Zhao[b]

School of Civil Engineering, Northwest Minzu University, Lanzhou, Gansu, China

[a]wuzhongtie1982@163.com,[b]2805103378@qq.com

Abstract. At present, with the rapid development and application of seismic isolation technology, compared with reinforced concrete columns, concrete-filled steel tube columns have superior mechanical properties such as high strength, light weight, good ductility, excellent bending performance, fatigue resistance and impact resistance. At present, the failure modes of series isolation components (SIS) composed of lead core rubber bearing (LRB) and steel tube concrete (CFST) columns are not studied. In order to have a deeper understanding of the failure mode of the series isolation components, 42 groups of refined SIS finite element models with h/b, n and α parameters were established using ABAQUS finite element software based on the 500mm diameter bearing model. By using Pushover analysis method, the relationship curve between force and displacement of series isolation system is studied, the damage process and failure mode of series isolation system are discussed, and the influence of three parameters on the failure mode is analyzed. The results show that the relationship between force and displacement of the new series isolation system is trilinear. The axial compression ratio mainly affects the bearing capacity of the steel pipe, and the higher the axial compression ratio, the smaller the bearing capacity. The aspect ratio and steel content mainly affect the stiffness and bearing capacity of the steel pipe. When the aspect ratio is less than or equal to 4.2 and the steel content is greater than or equal to 6.4%, the bearing capacity and stiffness are the best. The failure mode mainly includes the failure of connecting plate, the failure of bolt, the failure of concrete filled steel tube column and the failure of steel tube. The failure of concrete filled steel tube column is the main failure mode, and the standard design of concrete filled steel tube column should be strengthened.

Keywords: Series isolation system, CFST column, Pushover analysis, failure mode, parameter analysis Introduction.

1 Introduction

Concrete filled steel tube columns have superior mechanical properties such as high strength, light weight, good ductility, fatigue resistance and impact resistance, etc. In addition, they also have superior construction properties such as saving labor and materials, light erection and fast construction[1-4]. As one of the measures to prevent

Q. Gao et al. (eds.), *Proceedings of the 2024 7th International Conference on Structural Engineering and Industrial Architecture (ICSEIA 2024)*, Atlantis Highlights in Engineering 30,
https://doi.org/10.2991/978-94-6463-429-7_34

earthquakes in cities in earthquake protection areas, isolation technology has become the main means to improve the seismic toughness of single structures in the construction of resilient cities[5-6]. As a low layer isolation (referred to as series isolation structure) scheme, the isolation support (LRB) is placed between the top of the superstructure and the bottom cantilever column (CFST column) to form a series isolation composite component (SIS), as shown in Figure 1.

Compared with the foundation isolation scheme, it has the advantages of reducing the cost, good seismic performance and increasing the building space. In the past two years, a large number of engineering buildings have adopted this type of isolation scheme, which has potential application prospects.

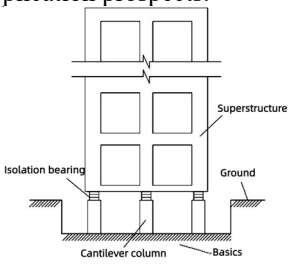

Fig. 1. Series isolation system[8]

Du Yong feng et al.[7] studied the nonlinear mechanical properties of SIS based on experiments and found that the nonlinear mechanical properties of SIS are mainly affected by the nonlinear mechanical properties of LRB and RC columns. Zhao Li jie et al.[8] conducted pseudo-static loading tests on series isolation components under different slenderness ratios and axial compression ratios, and found that the failure phenomena of the components were similar, and the transverse cracks were mainly concentrated in the area below 2/3 of the column height and were evenly distributed. Zhao Li jie et al.[9] conducted pseudo-static loading tests based on 5 groups of series isolation components with different coaxial pressure ratios and slenderness ratios, and found that the tensile and compressive damage of RC columns was mainly concentrated at the column roots. Huang Xiao ning et al.[10] proposed a new type of connection node suitable for RC series roller isolation structural column in view of the stress and damage characteristics of RC series roller isolation structure under earthquake action. Many studies have been done on the mechanical properties of concrete-filled steel tube [11]. Zhan Jie dong et al.[12] found that the damage form of the square specimen was four-sided bulge, while the round specimen changed from a cylinder to a barrel-like shape. Luo Shun xin et al.[13] used ABAQUS software to analyze the joint stress of eccentric joints of concrete-filled steel tubular columns and steel beams. Li Xue ping et al.[14] studied the effects of different test parameters (including axial compression ratio, section aspect ratio, steel content, loading direction, etc.) on the seismic performance of rectangular CFST columns. The research results of Wang Jing feng et al.[15] show that the failure modes of elliptical concrete-filled steel tubular columns mainly include local buckling and tearing of the steel tube at the foot of the column and core cement crushing

and other phenomena under horizontal and low cyclic cyclic loads. The failure mode analysis of LRB and CFST column isolation components in series is still lacking.

Therefore, on the basis of the above research, this paper completed the finite element simulation analysis of 35 groups of series isolation components with different aspect ratio, axial compression ratio and 7 groups with different steel content. The failure phenomena and characteristics of series isolation components under different aspect ratio, axial compression ratio and steel content are analyzed.

2 Establishment of Abaqus finite element model

2.1 Material Constituency and Unit Setting

In order to have a deeper understanding of the failure mode of the series isolation component, this paper uses the large general finite element software ABAQUS to establish the solid model of the series isolation component. The finite element model of series isolation component established by ABAQUS finite element software in this research project is shown in Figure 2. LRB dimensions are shown in Table 1 and CFST column dimensions are shown in Table 2. According to literature[16], the CDP model suitable for ABAQUS cyclic load is selected as the constitutive model of concrete. C3D8R unit is adopted. Poisson's ratio of concrete is set at 0.2, elastic modulus is 22980.7MPa, expansion Angle of concrete is 35°, and eccentricity of plastic potential function is 0.1. The ratio of biaxial ultimate compressive strength to uniaxial ultimate compressive strength of concrete is 1.16, the ratio of the second stress invariant of the tension and compression meridian is 0.667, and the viscosity coefficient is 0.005.Rubber adopts the two-constant constitutive model Mooney-Rivlin[17], in which the two constants are C_{10}=0.18MPa and C_{01}=0.045MPa respectively. The rubber adopts C3D8RH unit, the rubber hardness is 47.1 degrees Shore, the shear modulus G=0.45, the first shape coefficient S_1=25.2, the second shape coefficient S_2=5.3. The steel is made of C3D8R unit, the steel pipe, connecting plate and the inner connecting plate of the foundation beam are all Q345 steel, the yield strength of the steel is 305MPa, and the bolts are made of 8.8 M22 bolts, the yield strength of the bolts is 640MPa.

2.2 Interaction and boundary conditions

The contact surface between the steel pipe and the internal concrete adopts the face-surface contact, the tangential friction is expressed by the "penalty" friction formula, the friction coefficient is 0.6[18], the normal contact stress behavior is "hard contact", and the embedded steel ring on the top of the connecting plate and CFST column, the bottom end of the steel pipe and the foundation beam are defined by binding constraints. The bottom of SIS adopts fixed constraints, which do not allow translation and rotation, and the top of the support allows displacement and rotation in X, Y and Z directions.

2.3 Loading system and load setting

The displacement control loading system is used for Pushover analysis of the series components, and the unidirectional loading displacement ranges from 0 to 336mm (600% shear deformation of the support). The SIS is based on 500LRB diameter, and the lower section is fitted with CFST columns of different n, h/b and α dimensions of 500mm×500mm. There are 35 combined models of axial compression ratio and aspect ratio. There are 7 models with different α, which are SIS with the thickness of 4mm, 8mm, 10mm, 12mm, 14mm, 16mm and 18mm, respectively, when the aspect ratio is 3 and the axial pressure ratio is 0.243. The compressive stress limits of isolation supports under the representative value of gravity load are 10MPa, 12MPa and 15MPa respectively for special fortification buildings, key fortification buildings and standard fortification buildings. The vertical loads of 8MPa (low load) and 18MPa (high load) are added in this study. Shear deformation of 100% (force-proof earthquake), 250% (rare earthquake) and 400% (extremely rare earthquake) of LRB is the control index of the whole SIS. The effects of different aspect ratio, axial compression ratio 0.162 (vertical load 8MPa), 0.203 (10MPa), 0.243 (12MPa), 0.304 (15MPa), 0.365 (18MPa) and different steel content on the failure mode of SIS were investigated. The basic parameters and combination form of the model are shown in Table 1 to 2. n is the axial compression ratio, h/b is the aspect ratio, and α is the steel content.

Table 1. LRB parameters

h/mm	D_l/mm	T_s/mm	N_s/layer	T_r/mm	N_r/layer	T_{es}/mm	N_{es}/layer
164	100	2.27	18	4.9	19	15	2

Note: D_l is the diameter of the lead core; h is the height of the laminated rubber bearing; T_S is the thickness of the inner steel plate; N_S is the number of layers of the inner steel plate; T_r is the thickness of the rubber layer; N_r is the number of layers of rubber; T_{es} is the thickness of the sealing steel plate; N_{es} is the number of sealing steel plates.

Table 2. Geometric parameters of prefabricated CFST columns

Dimension		Column length						
h	b	L_1	L_2	L_3	L_4	L_5	L_6	L_7
500	500	1000	1500	1700	1900	2100	2500	3000

Note: L_i represents the length of the i-th column, where i ranges from 1 to 7; h is the cross-sectional height of the CFST column; b is the cross-sectional width of the CFST column.

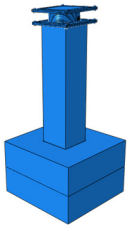

Fig. 2. SIS Finite Element Model Diagram

3 Finite element analysis results

3.1 Parameter verification analysis of lead rubber bearings

In order to ensure the rationality of parameters for the lead-core rubber bearing in a series isolation system, a finite element model was established based on relevant parameters from literature[19].The key mechanical parameters including yield force, equivalent stiffness, post-yield stiffness, and equivalent damping ratio were compared and analyzed.

The yield force, equivalent stiffness, post-yield stiffness, and equivalent damping ratio obtained from the hysteretic curve of the finite element simulation for a single rubber bearing (as shown in Figure 3 and Table 3) are slightly lower than the design values. However, these differences remain within a range of 10%, which effectively reflects the actual parameters of the lead core rubber bearing.

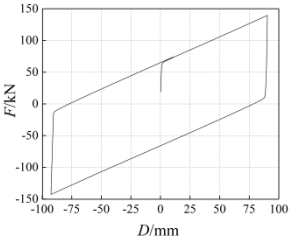

Fig. 3. Hysteresis curve of LRB shear deformation at 100%

Table 3. LRB parameter comparison

Shear deformation 100%	yield force (kN)	Equivalent Stiffness (kN/mm)	Post yield stiffness (kN/mm)	equivalent damping ratio(%)
Design value	65.3	1.62	0.91	26
analog value	64.5	1.54	0.84	24.6
error	1.2%	4.9%	7.6%	5.4%

3.2 The force-displacement curves of SIS

It can be seen from FIG. 4, 5 and 6 that the force-displacement variation relationship of SIS, LRB and CFST columns is an obvious nonlinear variation relationship, and the thrust curve of SIS presents a trilinear variation, in which the first yield point is the yield of LRB and the second yield point is the yield of CFST columns. Two yield points can divide the curve into three parts: initial section, first yield section and second yield section. It can be seen from FIG. 4, 5 and 6 that the yield points of CFST column are basically consistent with the two yield points of SIS, which more strongly indicates that the two yield points of SIS are caused by the yield of CFST column.

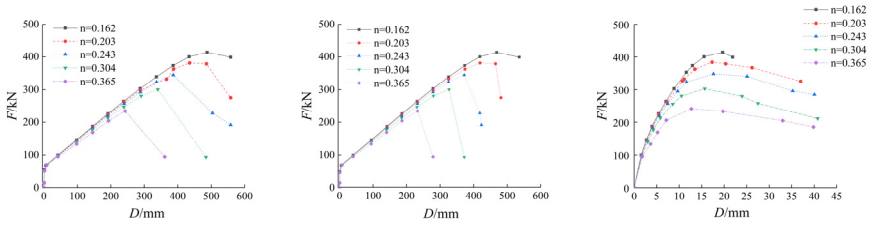

(a)SIS (b)LRB (c)CFST column

Fig. 4. h/b=3.8, α=6.4%, force and displacement curves under different n values

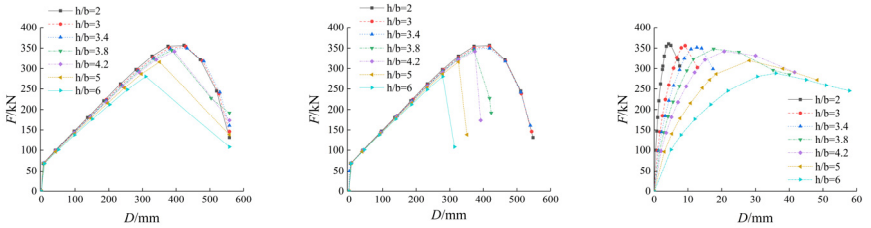

(a)SIS (b)LRB (c)CFST column

Fig. 5. Force and displacement curves at different h/b values, n=0.243(p=12MPa), α=6.4%

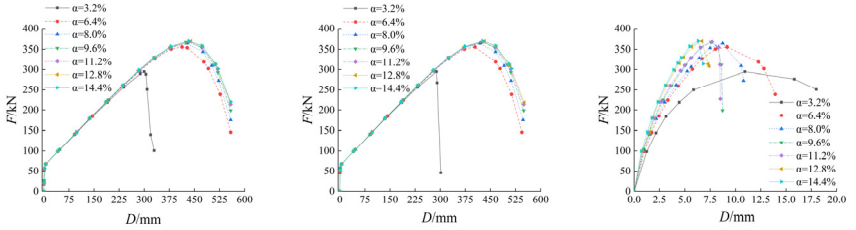

(a)SIS (b)LRB (c)CFST column

Fig. 6. h/b=3, n=0.243(p=12MPa), different α Force and displacement curve under

The bearing capacity of SIS, LRB, and CFST columns gradually decreases with an increase in the axial compression ratio of the system when the aspect ratio remains constant, as depicted in FIG. 4. The force-displacement curve of SIS exhibits a similar trend to that of LRB but differs from that of CFST column, indicating that variations in the force-displacement curve of SIS are primarily influenced by LRB when subjected to changes in axial compression ratio under identical aspect ratios. The results depicted in FIG. 5 demonstrate that, when the axial compression ratio remains constant, an increase in the aspect ratio of CFST columns leads to a decrease in column stiffness, earlier yielding of the column, and a gradual reduction in bearing capacity. Consequently, the bearing capacity of SIS gradually decreases with increasing aspect ratio. In FIG. 5, for aspect ratios below 4.2, SIS exhibits its highest load-bearing capacity and its force-displacement relationship curve aligns closely with that of LRB. This indicates that as the aspect ratio of CFST columns increases, their stiffness diminishes and

increasingly influences the force-displacement relationship curve of SIS. The variation in steel content primarily affects both the bearing capacity of SIS and the rigidity of CFST columns. As can be seen in Figure 6, when the steel content of the steel pipe is greater than or equal to 6.4% (thickness 8mm), the bearing capacity and column stiffness of SIS are the largest; when the α of CFST column is greater than or equal to 6.4% (thickness 8mm), the force-displacement relationship curve of SIS is basically consistent with the change trend of LRB. Therefore, with the increase of steel content of CFST column, the influence of LRB on the force-displacement relationship curve of SIS becomes more obvious.

3.3 Enhanced analysis of the impact of three parameters on failure mode

The SIS system primarily consists of CFST columns, LRBs, and connectors, thus its failure mode is predominantly determined by the failure mechanisms of these components. These include buckling of the CFST column steel pipe, drum bending, concrete crushing and cracking, as well as connector buckling failure. The failure sequence in SIS begins with yielding at the four corners of the lower end of the steel pipe, followed by tensile and compressive yielding of the connecting plate, and ultimately shear yielding of the bolt; however, no cracking occurs within the concrete encased in the steel pipe.

The bolt is extracted from the location where the stress on the lower connecting plate reaches its maximum, while the connecting plate is taken from the lower connecting plate of LRB. As depicted in Figure 7 (c) and (d), both bolts and connecting plates experience yield failure prior to n=0.243 and a shear deformation of 300% on the support. The bolt stress cloud diagram in Figure 8 reveals that shear failure predominantly occurs in bolts, which gradually weakens with an increase in aspect ratio. The stress cloud diagram of the connecting plate in Figure 8 demonstrates that compression failure initially occurs, followed by tensile yield failure as horizontal displacement of the support increases. The stress cloud diagram of the concrete column in Figure 8 indicates that concrete failure concentrates at both ends of the column, with SIS having h/b=3 failing at its upper end, while SIS with h/b=4.2 and 5 fail at their lower ends. The concrete inside CFST columns for all three SIS remains undamaged, without reaching its maximum cracking strain.

The CFST column is the most vulnerable component in SIS. Figure 7 (a) demonstrates that for a given axis n, an increase in the h/b ratio of the steel pipe leads to faster yielding. Similarly, Figure 7 (b) shows that for a constant n value, a larger h/b ratio results in earlier yield time. FIG. 9 and 10 depict stress cloud diagrams of the steel pipe within SIS. Considering the similarity in stress distribution and failure modes among steel tubes with different h/b and n values in SIS, only two diagrams are presented in FIG. 9 and 10. The stress cloud diagrams from FIG. 9 and 10 reveal that as horizontal displacement load increases, buckling failure initiates at the lower end of the steel pipe along the loading direction first, followed by buckling failure at the upper end. The yield area of the steel pipe gradually increases with an increase in n under the same h/b, as depicted in FIG. 9. Furthermore, the stress cloud diagram in Figure 10 reveals that for a constant n, the yield area at the upper end of the steel pipe progressively decreases

with an increase in h/b. It is noteworthy that when the aspect ratio exceeds 4.2, no damage occurs at the upper end of the steel pipe anymore. Therefore, for aspect ratios below 4.2, attention should be given to both upper and lower end yielding; whereas for aspect ratios above 4.2, emphasis should be placed on lower end yielding instead. Additionally, Figure 11 demonstrates that as α (steel pipe content) increases, there is a gradual reduction in yield area at the upper end of the steel pipe until it no longer yields at all when α reaches or exceeds 9.6%.

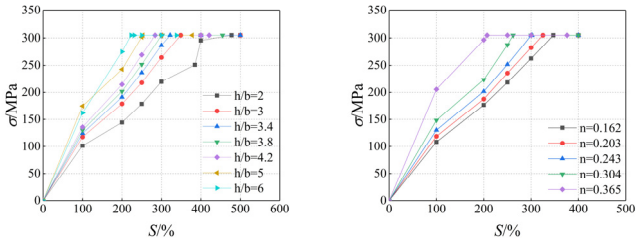

(a)steel pipe n=0.243(p=12MPa)(b)steel pipe h/b=3.8

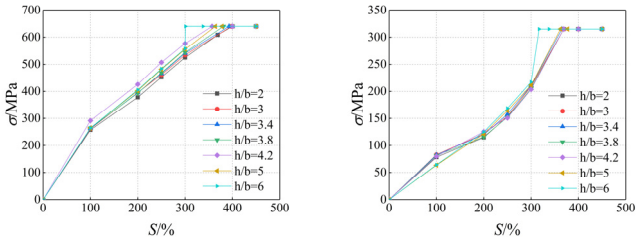

(c)bolt n=0.243(p=12MPa)(d)connecting plate n=0.243(p=12MPa)

Fig. 7. α=6.4%, the relationship between stress and shear deformation of rubber bearing curve

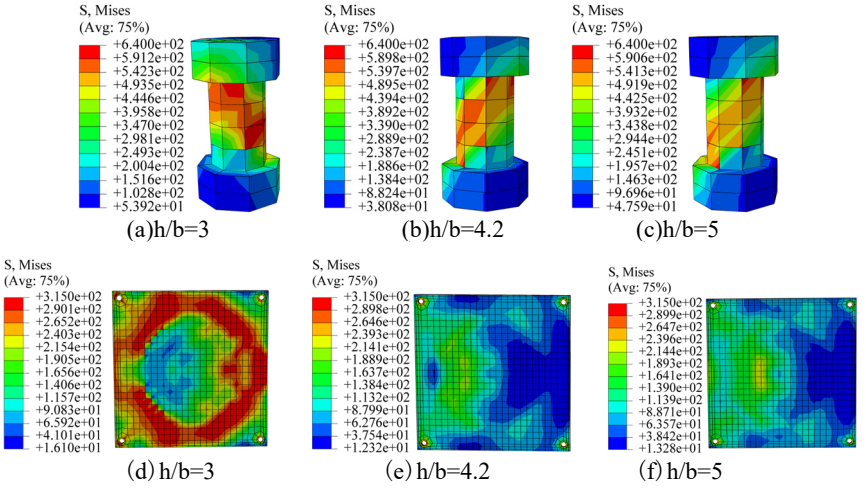

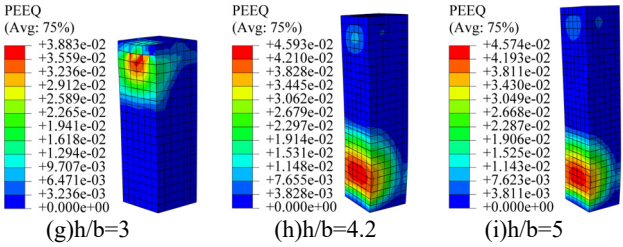

Fig. 8. Finite element simulation results of concrete inside bolts, connecting plates and steel tubes under α=6.4% and n=0.243

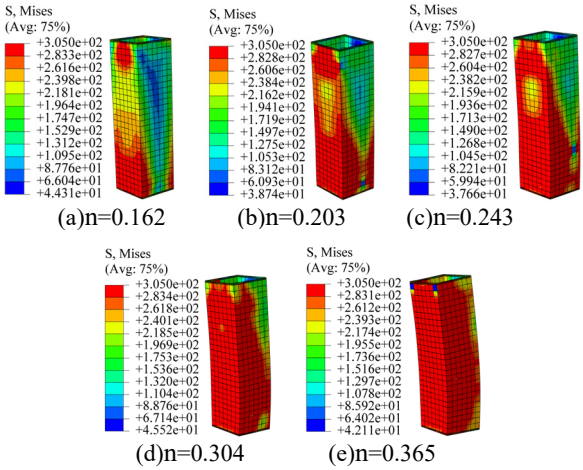

Fig. 9. Stress cloud map of steel pipes with different n values at h/b=3.8,α=6.4%

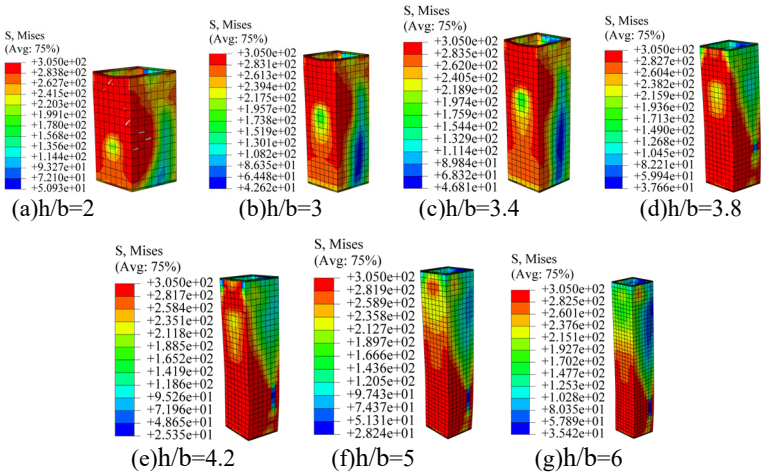

Fig. 10. Stress nephogram of steel pipe with different h/b at n=0.243, α=6.4%

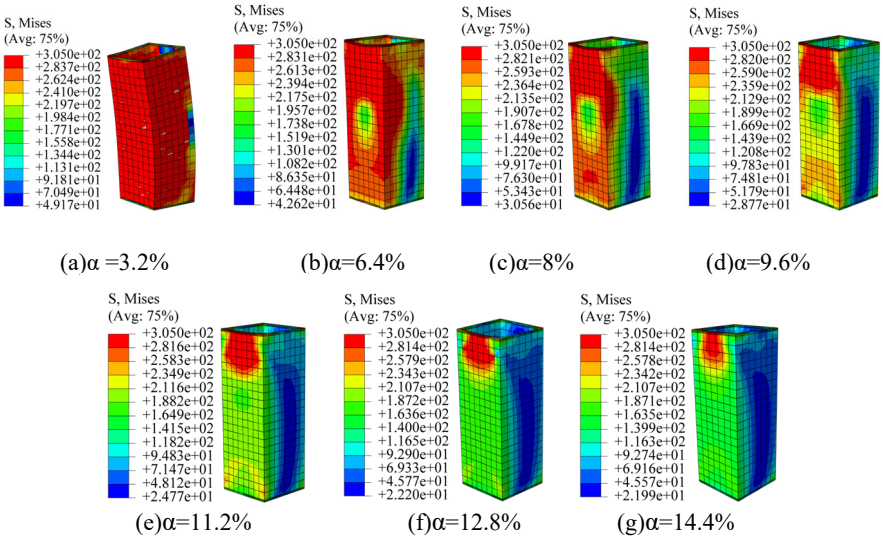

Fig. 11. Stress Cloud Map of Steel Pipe at h/b=3, n=0.243(p=12MPa)

4 Conclusions

The pushover analysis method is employed in this study to examine the failure mode of a novel series isolation system comprising rubber bearings and concrete-filled steel tube columns. The subsequent findings are as follows:

(1) The nappe curve of SIS is trilinear. When the aspect ratio and steel content are constant, the bearing capacity of SIS decreases gradually with the increase of axial compression ratio. When axial compression ratio and steel content are constant, the column stiffness decreases and the bearing capacity of SIS decreases with the increase of aspect ratio. When the ratio of height to width and axial compression is constant, the bearing capacity of SIS increases gradually with the increase of steel content. The mechanical properties of SIS are optimal when the ratio of height to width is less than or equal to 4.2 and the steel content is greater than or equal to 6.4%.

(2) The shear failure of bolts is mainly shear failure, and the shear failure of bolts is gradually weakened with the increase of aspect ratio. The buckling failure of the connecting plate is caused by the tension and compression of the support, and the failure weakens gradually with the increase of the aspect ratio. The failure of concrete is concentrated in the upper and lower ends of the column, and the compression failure. The failure point of the steel pipe is at both ends, mainly the buckling failure and tension failure.

(3)Under the same aspect ratio and steel content, the yield area of the steel pipe gradually increases with the increase of axial compression ratio. Under the same axial compression ratio and steel content, the yield area of the upper end of the steel pipe decreases gradually with the increase of the aspect ratio. Under the same aspect ratio and axial compression ratio, with the increase of α, the lower end of the steel pipe

gradually no longer yields, and only the upper end of the steel pipe has a buckling phenomenon.

(4)In the structural design, the height to width ratio and steel content of the column should be specified. According to the research in this paper, it is suggested to set the aspect ratio interval of CFST column to be less than or equal to 4.2, the steel content interval of steel pipe to be greater than or equal to 6.4%, and the mechanical properties of SIS are the best. There are still some shortcomings in the research content of this paper, and further research will be carried out.

Acknowledgments

The research presented in this article was supported by the National Natural Science Foundation of China (Project NO.51868067), the Special Fund for Basic Scientific Research of Central Universities (31920230181), the Natural Science Foundation of Gansu Province (Project NO.20JR5RA508), and the Innovation Fund of Gansu Universities (Project NO.2020B-067, and NO.2022B-248).

References

1. Gupta, P.K., Srd, S.M., Kumar, M.S. (2007) Experimental and computational study of concrete filled steel tubular columns under axial loads. J. Journal of Constructional Steel Research.Commun.,63(2):182. https://doi.org/10.1016/j.jcsr.2006.04.004.
2. Wang, F.Q., Liu, F.Q., Yang, H, et al. (2023) Axial compressive performances of thin-walled steel tube confined steel-reinforced concrete columns after fire exposure. J. Thin-Walled Struc-tures. Commun.,190:110919.https://doi.org/10.1016/j.tws.2023.110919.
3. Yuan,F., Li,Z.W., Li, H.H., et al. (2023) Effect of high-strength steel spirals on the seismic behavior of square concrete-filled steel tubular columns under high axial l oad ratio. J Engineering Struc-tures.Commun.,279:115652.https://doi.org/10.1016/j.engstruct.2023.115652.
4. Han, L.H. (2007) Concrete-filled steel tube structures-Theory and practice. Science Publishing, Beijing. BFE1BF225BBAA4F289B54EE7D2099B1E6000.pdf (ecsponline.com).
5. Yang, J., Li, D.P., Zhai, C.H., et al. (2019) Research status and key scientific issues of urban seismic toughness. J. Bulletin of National Natural Science Foundation of China, Commun.,33(5)525-532.10. https://doi.org/16262/j.cnki.1000-8217.2019.05.018.
6. Zhou, Y., Wu, H., Gu, A.Q. (2019) Earthquake engineering: from earthquake resista nce, energy disssiption, and isolation, to resilience. J. Engineering Mechanies, Com mun.,36(6):1-12.(cstam.org.cn).
7. Du, Y.F., Wu, Z.T., Zhu, Q.K. (2015) Finite element analysis of nonlinear mechanical properties of series isolation systems based on experiments. J. Journal of Civil Engineering. Commun.,48 (7): 23-26. https://doi.org/10.15951/j.tmgcxb.2015.07.003.
8. Zhao, L.J., Jing, H.G., Du, Y.F., Shen JS. (2023) Experimental study on nonlinear mechanical properties of series isolation components. J. Journal of Vibration and Shock. Commun.,42:24-25. https://doi.org/10.13465/j.cnki.jvs.2023.05.004.
9. Zhao, L.J., Zang, Z.H., Shen, J.S., Et al. (2023) Experimental study on restoring force calculation model of series isolation components. J. China Science paper. Commun.,18:359-361. https://www.nstl.gov.cn/paper_detail.html?id=b20510b09f6615739f87e5cab5e343b0.

10. Huang, X.N., He, T., Et al. (2023) Experimental study on seismic performance of asse mbled RC series roller isolation structure columns. J. Engineering Mechanics. Commu n.,40:93-96. https://www.zhangqiaokeyan.com/academic-journal-cn_detail_thesis/020121 01739859.html.
11. Schneider., Stephen, P. (1998) Axially loaded concrete-filled steel tubes. J. ASCE, Journal of Structural Engineering. Commun.,124(10): 1125-1138. Axially Loaded Concrete-Filled Steel Tubes | Journal of Structural Engineering | Vol 124, No 10 (ascelibrary.org).
12. Zhan, J.D., Wang, Y.K. (2024) Axial compression properties of concrete-filled steel tube columns with the same section area and different sections. J. Metallic Functional Materials. Commun.,31:61-62. https://doi.org/10.13228/j.boyuan.issn1005-8192.20230115.
13. Luo, S.X., Shen, Q., Et al (2023) Finite element analysis of eccentric joint between rectangular concrete-filled steel tube column and H-shaped steel beam. J. Building Structure. Commun.,53:1510-1512. https://doi.org/10.19701/j.jzjg.23S2233.
14. Li, X.P., Lv, X.L., Guo, S.C. (2005) Seismic performance of rectangular steel tube concrete columns under cyclic loading I: Experimental study. J. Earthquake Engineering and Engineering Dynamics.Commun.,25:98-02. https://doi.org/10.13197/j.eeev.2005.05.016.
15. Wang, J.F., Hua, Z.M., et al. (2023) Test and analysis of seismic performance of ellip tical concrete-filled steel tube columns. J. China Civil Engineering Journal. Commun., 56:41-42. https://doi.org/10.15951/j.tmgcxb.21121269.
16. Yao, F.B. (2019) Numerical simulation and seismic performance analysis of high-strength reinforced concrete columns based on ABAQUS. [D]. Hefei: Hefei University of Technology.Commun.,7-23. (caq98i.top).
17. Liu, M., Wang, Q.C., Wang, G.Q. (2011) Determination for material constants of rubb er Mooney-Rivlin model. J. China Rubber Industry, Commun.,58(4):241-245. www.cq vip.com.
18. Baltay, P., Gjelsvik, A. (1990) Coefficient of Friction for Steel on Concrete at High Normal Stress. J. Journal of Materials in Civil Engineering.Commun.,2(1):46-49. Coefficient of Friction for Steel on Concrete at High Normal Stress | Journal of Materials in Civil Engineering | Vol 2, No 1 (ascelibrary.org).
19. Dang, Y. (2007) Guidelines for Design and Construction of Basic Isolation Structures. China Water Power Press, The Beijing. https://xueshu.baidu.com/usercenter/paper/show?paperid=72d04ecf43b129ae8863514e3855115a&site=xueshu_se&hitarticle=1.